Pérez María Eugenia (Orcid ID: 0000-0003-2067-8954)
Durantini Andres Matias (Orcid ID: 0000-0002-7898-4033)
Durantini Edgardo N. N. (Orcid ID: 0000-0001-8901-7543)

Diketopyrrolopyrrole Derivatives as Photosensitizing Agents against *Staphylococcus Aureus*

María E. Pérez[1], Vitor A. S. Almodovar[2], Javier E. Durantini[3], Natalia S. Gsponer[1], Andrés M. Durantini[1], Augusto C. Tomé[2]* and Edgardo N. Durantini[1]*

[1] IDAS-CONICET, Departamento de Química, Facultad de Ciencias Exactas, Físico-Químicas y Naturales, Universidad Nacional de Río Cuarto, Ruta Nacional 36 Km 601, X5804BYA Río Cuarto, Córdoba, Argentina.

[2]LAQV-REQUIMTE, Department of Chemistry, University of Aveiro, 3810-193 Aveiro, Portugal.

[3] IITEMA-CONICET, Departamento de Química, Facultad de Ciencias Exactas, Físico-Químicas y Naturales, Universidad Nacional de Río Cuarto, Ruta Nacional 36 Km 601, X5804BYA Río Cuarto, Córdoba, Argentina.

* Corresponding author email: edurantini@exa.unrc.edu.ar (Edgardo N. Durantini), actome@ua.pt (Augusto C. Tomé)

This article has been accepted for publication and undergone full peer review but has not been through the copyediting, typesetting, pagination and proofreading process which may lead to differences between this version and the Version of Record. Please cite this article as doi: 10.1111/php.13741

ABSTRACT

Diketopyrrolopyrrole (DPP) derivatives containing sulfonamide (**Sulfonamide-DPP**), pyridyl (**Dipyridyl-DPP**) and *N*-methylpyridyl (**MePyridyl-DPP**) substituents were assessed as antibacterial photosensitizers. Non-charged DPPs showed an intense absorption band centered at about 480 nm and green fluorescence emission ($\Phi_F \sim 0.7$) in acetonitrile. The absorption of **MePyridyl-DPP** was bathochromically shifted at 510 nm, with decreased fluorescence emission. **Sulfonamide-DPP** and **Dipyridyl-DPP** photosensitized the formation of $O_2(^1\Delta_g)$ ($\Phi_\Delta \sim 0.15-0.17$), while the production induced by **MePyridyl-DPP** was at least 10 times lower. Furthermore, these DPPs produced a photoreduction of NBT similar to that of the control. Photodynamic inactivation induced by DPPs was first investigated at single-bacterium level of *Staphylococcus aureus* attached to a surface. After 30 min irradiation, **MePyridyl-DPP** produced a complete eradication of the bacteria. In bacterial cell suspensions, dicationic DPP induced more than 7 $\log_{10}$ decrease in *S. aureus* cell survival after 30 min irradiation. Potentiation with iodide anions allowed a complete elimination of bacteria after 15 min therapy. This compound was also effective to eliminate *S. aureus* cells on biofilms. The results show that **MePyridyl-DPP** bearing two positive groups provides an amphiphilic character to the structure that improves the interaction with the cell envelop. This effect enhances the photocytotoxic activity of **MePyridyl-DPP** against bacteria.

Keywords: diketopyrrolopyrrole; photodynamic inactivation; reactive oxygen species; photoinactivation; microorganism.

INTRODUCTION

Photodynamic therapy (PDT) represents an interesting approach for the treatment of neoplastic tissues (1). This technique is currently being extended to several non-cancerous illnesses, especially those characterized by unwanted cell overgrowth, such as various dermatological diseases, benign prostatic hyperplasia and age-related macular degenerations. In the last decades, research and development in this field have allowed the use of photosensitizers (PSs) in the treatment of infectious diseases (2). This procedure is named photodynamic inactivation (PDI) of microorganisms. In this sense, the PDI could become a solution for this type of health problems. PDI therapy is based on the following central stages, which can be numbered as the selective accumulation of the PS in the microbial cells, the irradiation of the affected area to produce reactive oxygen species (ROS), and the reaction of these ROS with the macromolecules of the cells causing lethal damage to microbes (3). Therefore, this therapy represents an interesting alternative to conventional antibiotics for the treatment of various infectious diseases (4).

A wide variety of PSs, such as derivatives of porphyrins, chlorins, bacteriochlorins, phthalocyanines, and fullerenes, have been proposed as potential phototherapeutic agents (5- 9). In addition, smaller structures containing two pyrrole units, such as BODIPYs, have been effective agents for the induced inactivation of bacteria (10,11). In this sense, diketopyrrolopyrroles (DPPs, 2,5-dihydropyrrolo[4,3-*c*] pyrrolo-1,4-diones) are a family of small molecules with a planar structure that can induce strong π–π stacking with neighboring molecules and intermolecular hydrogen bonding (12). These heterocycles represent a class of brilliant red and strong fluorescent high-performance dyes and pigments, which attracted wide attention in recent years due to their interesting properties. The high fluorescence emission, the low photobleaching, and environment and thermal stability makes DPPs excellent candidates as fluorescent sensors (13,14). Thus, flexible fluorescent DPP-based ionic liquid derivatives were evaluated as effective antibacterial agents (15). The potential biological application of DPPs as phototherapeutic agents in PDT was reported in recent years (16). Additionally, due to their chemical stability and solubility in aqueous media, these molecules were

also described as good fluorescent DNA biosensors (17). DPP-containing conjugated polymers were explored as antibacterial nanoparticles by combining photothermal therapy and PDT (18). Also, a DPP-based conjugated polymer was assessed as photocatalyst to improve sterilization and degradation of organic pollutants (19). DPP derivatives alone present a very poor ISC, therefore different approaches were developed to mimic the heavy atom effect. In this context, DPP dyes can act as light-harvesting antenna in donor-C_{60} systems to generate efficient heavy atom-free triplet PSs (20).

In this work, DPP derivatives bearing sulfonamide (**Sulfonamide-DPP**), pyridyl (**Dipyridyl-DPP**) and *N*-methylpyridyl (**MePyridyl-DPP**) substituents (Scheme 1) were evaluated as potential phototherapeutic agents to inactivate bacteria. As observed for other PSs, the amphiphilic character of DPP structures can enhance their interaction with the cell membrane (10). Furthermore, the presence of cationic groups in the DPP periphery can be used to obtain a higher accumulation in the microbial cells (21,22). Spectroscopic characteristics of DPP derivatives were determined in solution and photodynamic properties were investigated in presence of different molecular probes to sense the formation of ROS. Recently, it was demonstrated that **MePyridyl-DPP** presents high affinity to G-quadruplex structures and is particularly selective for oncogene promotors (23). Herein, antimicrobial activity sensitized by these DPPs was studied in a Gram-positive bacterium *Staphylococcus aureus*. This microorganism was chosen because *S. aureus* is the main cause of bacterial infections in humans around the world (24,25). Although some PDI studies were performed mainly with polymeric derivatives or conjugates of DPPs, these studies represent the first investigations using molecular monomers, in particular a dicationic structure. Furthermore, in order to improve the eradication of pathogenic bacteria, the PDI of *S. aureus* was investigated using a combination of DPP plus KI.

<Scheme 1>

MATERIALS AND METHODS

Materials, instrumentation, computational details, growth conditions of bacterial strain and statistical analysis are detailed in the Supporting Information.

Synthesis of DPPs. **Dipyridyl-DPP** and **MePyridyl-DPP** were synthesized as reported (23). 2,5-Bis(2-ethylhexyl)-3,6-diphenyl-2,5-dihydropyrrolo[3,4-*c*]pyrrole-1,4-dione (DPP **2**, Scheme 2). A suspension of the DPP **1** (500 mg, 1.73 mmol) and K_2CO_3 (1.4 g, 10.4 mmol) in DMSO (60 mL) was heated at 65 °C under a nitrogen atmosphere for 30 min. At this temperature and under stirring, a solution of 3-(bromomethyl)heptane (1.8 mL, 10.4 mmol) in DMSO (8 mL) was added dropwise. Then, KI (700 mg) was added and the mixture was stirred overnight at 80 °C. After cooling to ambient temperature, the mixture was diluted with ethyl acetate and water. The organic layer was separated and washed with water and brine. The product (325 mg, 37% yield) was isolated by column chromatography (silica gel) using CH_2Cl_2 as the eluent. The ^1H and ^{13}C NMR spectra are identical to those previously reported (26). Mp: 169.8–170.7 ºC. ^1H NMR (300 MHz, $CDCl_3$) δ (ppm) 0.69 (t, J = 7.41 Hz, 6H), 0.77 (t, J = 6.7 Hz, 6H), 1.07–1.23 (m, 16H), 1.43–1.48 (m, 2H), 3.67–3.80 (m, 4H), 7.49–7.56 (m, 6H), 7.74–7.80 (m, 4H). ^{13}C NMR (75 MHz, $CDCl_3$) δ (ppm) 10.4, 13.9, 22.8, 23.7, 28.2, 30.3, 38.5, 44.9, 109.76, 126.6, 128.8, 130.9, 148.7, 162.8. MS (TOF): *m/z* 513.1 $(M+H)^+$.

Sulfonamide-DPP. DPP **2** (150 mg, 0.3 mmol) was slowly added to chlorosulfonic acid (0.24 mL, 3.5 mmol) at 0 °C. Then, the mixture was stirred for 1 h at ambient temperature and $SOCl_2$ (0.014 mL, 0.20 mmol) was added to the reaction mixture and it was stirred for 1 h at room temperature and 1 h at 50 ºC. After cooling to ambient temperature, the reaction mixture was slowly poured onto ice. The reaction product was extracted with CH_2Cl_2 and the organic phase was added to a solution of diethylamine (0.25 mL, 2.1 mmol) in CH_2Cl_2 (30 mL). The resulting mixture was stirred for one day at room temperature. The reaction mixture was washed with water (3 x 20 ml), the organic phase was dried over anhydrous sodium sulfate, and the solvent was evaporated under reduced pressure. The crude product was purified by preparative TLC (silica gel) using CH_2Cl_2 as the eluent. The

Sulfonamide-DPP was precipitated from CH_2Cl_2 by addition of hexane. After filtration and drying, a violet solid (30 mg, 13% yield) with mp 171–173 ºC was obtained. ^{1}H NMR (300 MHz, $CDCl_3$) δ (ppm) 0.69 (t, J = 7.43, 6H), 0.80 (t, J = 6.95, 6H), 1.04−1.22 (m, 28H), 1.38–1.47 (m, 2H), 3.29 (q, 8H), 3.73 (d, J = 7.38 Hz, 4H), 7.88–7.92 (m, 4H), 7.95–7.98 (m, 4H). ^{13}C NMR (75 MHz, $CDCl_3$) δ (ppm) 10.3, 13.9, 14.3, 22.8, 23.6, 28.2, 30.2, 38.7, 42.3, 45.2, 110.8, 127.5, 129.2, 131.9, 142.6, 147.5, 162.3. MS (TOF): *m/z* 783.4 $(M+H)^+$.

Spectroscopic studies. UV-visible absorption and fluorescence spectra were performed in acetonitrile (ACN) and *N*,*N*-dimethylformamide (DMF) using a quartz cell of 1 cm path length at room temperature. Absorbances of 0.05 of the DPP derivatives were matched at the excitation wavelength (λ_{exc} = 483 nm) and the areas of the emission spectra were recorded between 500 to 750 nm (20). The fluorescence quantum yield (Φ_F) was calculated by comparing the area under the corrected emission spectrum for each DPP with that corresponding to the reference (8-acetoxymethyl-1,3,5,7-tetramethyl pyrromethene fluoroborate, **H_2B-OAc**, Φ_F = 0.87) in the same solvent (27).

Photosensitized decomposition of 9,10-dimethylanthracene (DMA). Samples of DMA (35 μM) and DPP (A = 0.15 at 523 nm) in ACN (2 mL) were irradiated with light at λ_{irr} = 523 nm in a quartz cell of 1 cm path length. DMA photooxidation was monitored by the decreasing of the absorbance at λ_{max} = 376 nm (Figure S1). The observed rate constants of DMA (k_{obs}^{DMA}) degradation were calculated by a linear least-squares fit of the pseudo-first order kinetic plots of $\ln(A_0/A)$ *vs*. time (21). Quantum yields of $O_2(^1\Delta_g)$ production (Φ_Δ) were obtained by comparing the k_{obs}^{DMA} for the DPP with that for the reference (8-acetoxymethyl-2,6-dibromo-1,3,5,7-tetramethyl pyrromethene fluoroborate, **Br_2B-OAc**, Φ_Δ = 0.79) (27). Photooxidation of DMA sensitized by **MePyridyl-DPP** in methanol was performed as described above using Rose bengal as a reference (Φ_Δ = 0.76) (28).

Reduction of nitro blue tetrazolium (NBT). Stock solutions of 8 mM NBT and 20 mM NADH were prepared in water. The NBT method to sensed $O_2^{\cdot -}$ formation was achieved using 0.2 mM NBT, 0.5 mM NADH and DPP derivatives (A = 0.25 at 523 nm) in 2 mL of DMF/water (5%). Solutions were irradiated with light at 523 nm and the development of the reaction was observed by the increase of the absorbance at 560 nm (Figure S2) (22). Control experiments were performed using a solution containing NBT and NADH without DPP derivatives.

Photoinactivation at the single-bacterium level. Fluorescence microscopy investigations were carried out using the methodology previously reported (29,30). *S. aureus* was aerobically grown in tryptic soy agar for 18 h at 37 °C. After that, a single colony was selected and cultured overnight in tryptic soy agar. Bacterial samples were collected from the agar upon adding PBS (1 mL) and removing the agar streaks. Then, 1 mL of *S. aureus* suspension was incubated for 30 min at 37 °C in a chamber composed of a polymeric cylinder glue to a coverslip. This method allows bacterial cells to adhere to the glass surface. Unbound bacteria were removed from the chamber by washing with PBS. Bioimaging experiments were performed adding 583 μL of PBS and propidium iodide ($[PI]_{\text{in chamber}}$ =1 μM) to cells attached to glass the surface of the chamber. Cells were incubated for 15 min in the dark. Then 12 μL of PS was added ($[PS]_{\text{in chamber}}$ = 2 μM) and the bacteria incubated for another 20 min in the dark. Photoinactivation assays were performed with green light using a band pass filter (515/35) measured out of the objective. The fluence rate measured out of the objective was 1.0 mW/cm^2. Fluorescence images of PI were obtained using an emission band pass filter (645/75). For each imaging region, a brightfield image was acquired to check bacterial cells. Images were collected using a 100× magnification objective and captured by a CMOS camera.

Photoinactivation of planktonic bacteria. Growth conditions of *S. aureus* strain and statistical analysis are detailed in Supporting Information. *S. aureus* cell suspensions in PBS (2 mL, ~10^8 CFU/mL) were incubated with 2.0 μM DPP in Pyrex culture tubes (13x100 mm) for 20 min in the

dark at 37 °C (31,32). DPPs were added from 1.0 mM stock solutions in DMF. After that, 200 μL of the cell suspensions were transferred to each well of 96-well microtiter plate. The cultures were irradiated for different times (5, 15 and 30 min) with light-emitting diode (LED) array that emitted green light at 502 nm (2 mW/cm^2). A similar procedure was used to determine the PDI in the presence of 50 mM KI. The inorganic salt was added from 1.0 M aqueous stock solution. Microbial cells were incubated with KI for 10 min in the dark at 37°C and, after that, cells were treated with DPP as described above. Viable microbial cells were quantified by the spread plate technique using serial dilutions 10-fold in PBS. Each sample was streaked on tryptic soy agar plates in triplicate. The number of colonies was calculated after incubation of the plates for 24 h at 37 °C in the dark.

Photoinactivation on biofilm. Overnight culture of *S. aureus* was diluted in tryptic soy broth to obtain A = 0.4 at 660 nm (33). Then, 100 μL of this cell suspension were transferred to each well of 24-well microtiter plate containing an acrylic disc submerged in 2.1 mL of the culture medium with 1.1% glucose. The plate was incubated overnight with shaking (100 rpm) at 37°C. Discs with the biofilm were removed and washed twice with 2 mL PBS. After that, discs were placed in 1.9 mL PBS and incubated with 5 μM **MePyridyl-DPP** for 20 min in the dark at 37 °C. Plate was irradiated as described for planktonic bacteria for different periods. Each disc was transferred to a tube (13x100 mm) containing 2 ml PBS and the bacterial cells were suspended by vortexing for 5 min. Viable microbial cells were determined as described for planktonic cells.

RESULTS AND DISCUSSION

Synthesis of DPP derivatives

The three PSs used in this work were synthesized from 3,6-diphenyl-2,5-dihydropyrrolo[3,4-*c*]pyrrole-1,4-dione (DPP **1**, Scheme 2) and Pigment red 254 (Scheme S1), two commercially available DPP pigments. The **Sulfonamide-DPP** derivative was obtained in three steps from DPP **1** (Scheme 2), being the first step its *N*,*N'*-dialkylation with 3-(bromomethyl)heptane using a variation

of methods reported in the literature (26,34). The *N*,*N'*-bis(2-ethylhexyl)-DPP **2** was then submitted to chlorosulfonation with chlorosulfonic acid and thionyl chloride using a variation of the method reported for the chlorosulfonation of the *N*-unsubstituted pigment **1** (35). After isolation by extraction, the resulting chlorosulfonyl derivative **3** was converted immediately into **Sulfonamide-DPP** by reaction with diethylamine. The crude product was purified by preparative TLC (silica gel), which revealed the formation of several minor products, and the main fraction was isolated and identified by NMR and MS as the expected sulfonamide. The formation of **Sulfonamide-DPP** in low yield (13%), as well the low yields reported for similar sulfonamides (35), reveals that the DPP system is not very stable under the acidic conditions required for the chlorosulfonation.

Dipyridyl-DPP and the corresponding dicationic derivative **MePyridyl-DPP** were synthesized as recently reported (Scheme S1) (23). Dipyridyl-DPP was obtained from Pigment red 254 and 4-pyridylboronic acid, under Suzuki–Miyaura conditions, following a recently reported procedure (36).

<Scheme 2>

The substituents inserted at the *para*-position of the 3,6-diaryl groups of DPPs were used to change the charge density distribution and the amphiphilic character of the structures. To evaluate this effect, DPPs were optimized to a stationary point on the Born-Oppenheimer potential energy surface of the molecular structures (21,22). Figure 1 shows the optimized structures of DPPs and ESP surfaces for the ground state. DPP core has a planar structure with the phenylene group in an almost perpendicular arrangement. From this analysis, spatial regions in the molecular structure were determined indicating negative and positive molecular electrostatic potential. These surfaces indicate the relative locations of positive and negative charges that were colored blue and red, respectively. This study allowed visualizing the charged regions of each molecule and the distribution in the structure of the DPP derivatives. As can be observed, non-charged **Sulfonamide-DPP** and **Dipyridyl-**

DPP structures showed an almost homogeneous charge distribution, with a slight negative area on the oxygen atoms. Positive charge distributions for **MePyridyl-DPP** was placed around the ammonium groups. Furthermore, this cationic compound showed that positive charges are highly exposed at the peripheries of the DPP core. These results indicate that **MePyridyl-DPP** can present a high specific electrostatic interaction with the cell wall of microbial cells (21). The combination of the hydrophobic substituents and hydrophilic cationic groups in the DPP structure produces an intramolecular polarity axis. Thus, the dipole moment (μ) of DPPs was calculated to estimate the effect induced by the substituents upon the intramolecular polarity (Figure S3). A negligible value was determined for **Sulfonamide-DPP** and **Dipyridyl-DPP**. In contrast, **MePyridyl-DPP** presented a value of about 8.31 D. Therefore, the two cationic groups attached to the periphery of **MePyridyl-DPP** significantly increases the value of μ with respect to the non-charged DPPs. The amphiphilic character of these PSs can facilitate the penetration through the cell membrane, producing a better accumulation in the cells and consequently increasing the PDI of the microorganisms (22).

<Figure 1>

Absorption and fluorescence spectroscopic properties

The UV-visible absorption spectra of DPPs in ACN are shown in Fig. 2A. The corresponding spectroscopic data are listed in Table 1. The spectra of **Sulfonamide-DPP** and **Dipyridyl-DPP** are characterized by a band in the UV region, approximately at 290 nm, and another broad absorption band in the visible, centered at about 480 nm (14). In the case of **MePyridyl-DPP**, both bands are bathochromically shifted compared with those of **Dipyridyl-DPP** by 28 nm and 24 nm, respectively. Similar spectroscopic results were found for these DPPs in DMF (Figure S4).

The highest occupied molecular orbital (HOMO) and the lowest unoccupied molecular orbital (LUMO) of DPPs are illustrated in Fig. 3. These orbitals were calculated by DFT at the CAM-B3LYP/6–31G(d) level using Gaussian 09. The HOMO of these compounds was formed by π orbitals

concentrated at the DPP unit. In contrast, the LUMO is mostly localized among the peripheral aromatic moieties (37). Furthermore, the calculated orbitals exhibited that the presence of substituent groups produced a slightly effect on the optimized structure of the DPP core.

The fluorescence emission spectra of DPPs in ACN are shown in the Fig. 2B. The spectra of **Sulfonamide-DPP** and **Dipyridyl-DPP** present the characteristic band of substituted DPPs, which is centered around 560 nm (Table 1) (14). **MePyridyl-DPP** showed a bathochromic shift of 83 nm relative to the emission band of **Dipyridyl-DPP**. Considering these results, Stokes shifts were calculated from the absorption and fluorescence maxima of the DPPs bands. Large Stokes shifts of 76 nm and 80 nm were found for **Sulfonamide-DPP** and **Dipyridyl-DPP**, respectively. Furthermore, a value of 139 nm was obtained for **MePyridyl-DPP** in ACN. This behavior was also observed in DMF (Figure S4). To characterize the conformational changes of DPPs molecules due to excitation, the geometry of the lowest excited state S_1 was optimized at TD-DFT to find the minimum energy point in the excited state potential energy surface. The comparison between both the ground state (S_0) and excited state (S_1) geometries indicated a planarization of the aromatic system (Figure S5). The angles between the π-system of the peripheral aromatic rings with the central DPP unit change by 17.22°, 9.25° and 13.52° for **Sulfonamide-DPP**, **Dipyridyl-DPP** and **MePyridyl-DPP**, respectively. These modifications are accompanied by changes between the pyridyl substituents and the phenyl ring approaching coplanarity as the angles decrease by 5.03° for **Dipyridyl-DPP** and 8.23° for **MePyridyl-DPP**. Moreover, the values of Φ_F of these DPPs were determined in ACN (Table 1). Both non-charged DPPs showed high Φ_F values, which agree with those previously reported for similar structures in organic solvents (12,13). A lower fluorescence emission was detected for **MePyridyl-DPP**, possibly due to a partial aggregation of this dicationic DPP in ACN.

<Figure 2>

<Table 1>

<Figure 3>

Photooxidation of DMA

Generation of $O_2(^1\Delta_g)$ induced by DPPs were compared with that produced by **Br_2B-OAc**, using DMA as molecular probe in ACN (27). This anthracene substrate mainly quenches $O_2(^1\Delta_g)$ by chemical reaction to form the corresponding 9,10-endoperoxide (38). The samples were irradiated at 523 nm under aerobic conditions and the photooxidation of DMA was monitored by the decreasing of absorbance at λ_{max} = 376 nm (Figure S1). Photooxidation of DMA followed a pseudo first order kinetic at a wavelength of 376 nm with respect to the DMA concentration (Fig. 4). The values of k_{obs}^{DMA} sensitized by DPPs are summarized in Table 2. These results were used to determine the production $O_2(^1\Delta_g)$ by comparing the slope obtained for each PS with the value corresponding to the reference, **Br_2B-OAc** (27). Similar Φ_Δ values were found for **Sulfonamide-DPP** and **Dipyridyl-DPP** in ACN (Table 2). The production of $O_2(^1\Delta_g)$ sensitized by these compounds was consistent with those previously reported for structurally related DPPs (16). A lower Φ_Δ value was found for **MePyridyl-DPP**, which may not be completely dissolved as monomer in ACN. The formation of aggregates precludes the photodynamic activity decreasing the production of ROS. However, the photodynamic effect can change considerably in a structured cell microenvironment with respect to that obtained in solution (39). Furthermore, photooxidation od DMA sensitized by **MePyridyl-DPP** was determined in methanol (Figure S6). This polar solvent allows a better solubilization as monomer of the dicationic DPP. As can be seen in Table 2, in this medium the Φ_Δ value for **MePyridyl-DPP** was similar to those found for **Sulfonamide-DPP** and **Dipyridyl-DPP** in ACN. It was also previously established, using DMA as molecular probe, that DPP derivatives produce $O_2(^1\Delta_g)$ [40].

<Figure 4>

<Table 2>

Photosensitized reduction of NBT

The ability of DPPs to produce $O_2^{\cdot-}$ by type I mechanism was explored in DMF. For this purpose, DPPs were irradiated with light at 523 nm under aerobic conditions in solutions containing NBT and NADH. It is expected that the electron transfer type of reaction preferentially occurs in polar solvents, mainly with the incidence of the reducing agent NADH (22,38). Also, this organic solvent was chosen to allow an adequate solubilization of the reagents. The reaction of NBT with $O_2^{\cdot-}$ produces formazan, which can be monitored following the absorption band of the product centered around 560 nm (Figure S2) (22,32). The formation of $O_2^{\cdot-}$ detected by the NBT is shown in Fig. 5. These results indicate that the production of $O_2^{\cdot-}$ by DPPs and control was quite similar. Therefore, even though these DPPs present a low production of $O_2(^1\Delta_g)$ in solution, these compounds were also unable of sensitizing the formation of $O_2^{\cdot-}$ with the addition of NADH.

<Figure 5>

PDI of *S. aureus* on surfaces

DPP-sensitized PDI was first examined by inspecting individual bacteria under a fluorescence microscope. For this purpose, *S. aureus* cells were adhered to the surface of a coverslip in a circular chamber, following the previously described methodology (29,30). This experimental approach was based on the presence of bacterial pili, which help bacterial attachment to a surface (41). Fluorescence images were compared with phase contrast photographs to confirm the presence and position of bacteria on surfaces (Fig. 6). After incubation of the individual *S. aureus* cells with 1 μM PI for 15 min, bacteria were treated with 2 μM DPP in PBS for another 20 min in the dark. PI binds to DNA by intercalating between bases after cell membrane rupture. In aqueous solution, PI has a low red emission (Φ_F ~0.01), however, upon PI binding to DNA this emission value can increase up to 30-fold (42). Therefore, this fluorophore was used as a cell death marker for the bacteria bound in the chamber (43).

For PDI experiments at the single-bacterium level, cells were irradiated with green light coming from the microscope source for different times. Figure 6 shows the progress in PDI therapy sensitized by DPPs, as well as the control after different irradiation times between 0 and 30 min (1.8 J/cm^2). Control experiments of cells irradiated in the absence of DPP showed no significant cell damage after 30 min of irradiation (Fig. 6, last row). In contrast, photodamage of *S. aureus* cells was characterized by an increase in red fluorescence of the cell death marker. Under these experimental conditions, a negligible red fluorescence emission was found for cells treated with **Sulfonamide-DPP** (Fig. 6, first row), while **Dipyridyl-DPP** was able to produce an inactivation of about 68% (Fig. 6, second row). Of the three DPPs evaluated, **MePyridyl-DPP** was the most effective PS to kill *S. aureus*, reaching an inactivation greater than 95% after 30 min irradiation (Fig. 6, third row). Previously it was observed that a cationic BODIPY, with low $O_2(^1\Delta_g)$ production in solution, was effective in eliminating *S. aureus* bound to a surface with similar characteristics (29). Furthermore, BODIPYs conjugated with iron oxide magnetic nanoparticles were able to photoinactivate *S. aureus* at the single bacterium level (44). Therefore, these results indicate that this dicationic DPP was an effective PS in photoinactivating bacteria attached to a surface, which represent an oversimplified example of a first stage of biofilm formation (45).

<Figure 6>

PDI of *S. aureus* cell suspensions

Photoinactivation induced by DPPs was also investigated in *S. aureus* cell suspensions (~10^8 CFU/mL). This microbial strain was selected because it may cause pathogenic diseases in humans (24). Microorganism cultures suspended in PBS were treated with 2.0 μM DPP for 20 min at 37 °C in the dark. Subsequently, the cells were exposed to green light for different times (5, 15 and 30 min, which signify 0.6, 1.8 and 3.6 J/cm^2, respectively). At this concentration, the DPPs were not toxic to

the microbial cells for 30 min incubation in the dark (Figure S7). Moreover, the viability of the bacteria was not affected by cell irradiation without DPP (Fig. 7). Therefore, PDI of cultures observed after irradiation of the *S. aureus* cells treated with DPPs was produced by the photodynamic activity sensitized by these compounds. Survival of microbial cells after different PDI treatments are shown in Fig. 7. Cell viability depended on both the DPP derivatives and the times of exposure to green light. After 30 min irradiation, 1 $\log_{10}$ decrease in bacterial survival was found in *S. aureus* cells treated with 2.0 μM **Sulfonamide-DPP** or **Dipyridyl-DPP**. However, the photokilling activity induced by **MePyridyl-DPP** was higher, reaching over 7 $\log_{10}$ of cell inactivation. The reduction in viability produced by the dicationic DPP represented a value greater than 99.9999% of cell inactivation. Furthermore, **MePyridyl-DPP** showed a photodynamic effect of 3 $\log_{10}$ (99.9%) and 4.4 $\log_{10}$ reduction (99.99%) after 5 min and 15 min irradiation, respectively. In previous investigations, two cationic BODIPY derivatives with low $O_2(^1\Delta_g)$ production were evaluated as PSs to inactivate *S. aureus* (46). Similar cell inactivation results were found but using white light with a fluence of 63 J/cm^2. Herein, **MePyridyl-DPP** was effective to eliminate this Gram-positive bacterium irradiated with green light of 3.6 J/cm^2.

<Figure 7>

On the other hand, PDI of *S. aureus* induced by these DPPs was examined in the presence of KI. In several cases, PDI can be potentiated by the addition of simple inorganic salts, being KI one of the most versatile (47). Consequently, *S. aureus* cells were treated with 50 mM KI before adding the PS. This concentration of KI was selected considering previous reports for the potentiation of PDI (38,39). This inorganic salt was not toxic to microorganisms exposed to irradiation for 30 min (Fig. 8). Furthermore, the treatment with 50 mM KI and 2 μM DPP was not toxic to the cells incubated in the dark (Figure S8). As expected, for the three DPPs the addition of KI caused an increase in the photokilling of *S. aureus* (Fig. 8). The combined therapy photosensitized by **Sulfonamide-DPP** and

Dipyridyl-DPP produced about 2 $\log_{10}$ decrease in the cell survival after 30 min irradiation. Most importantly, the presence of KI considerably improved the PDI induced by **MePyridyl-DPP**, reaching a reduction of 6 $\log_{10}$ after 5 min irradiation. Under these conditions, a complete eradication of the bacteria was achieved after irradiation for 15 min. It was reported that the efficacy of PDI mediated by methylene blue was considerably increased in *S. aureus* by addition of KI (48). Also, PDI of bacteria sensitized by cationic fullerenes was potentiated by iodide anions (38,49). Potentiation by iodide anions was also used to improve the PDI of microorganisms induced by several cationic and anionic porphyrins (31,50-52). This inorganic salt was also able to enhance the photoinactivation of microorganisms sensitized by BODIPYs, which similarly to DPPs have a low production of $O_2(^1\Delta_g)$ (39,46). Iodide anions can increase the rate of intersystem crossing of many dyes to form triplet excited states by the external heavy-atom effect (39,53). Moreover, reactive iodine species can be formed in an aqueous media (Scheme S2) (54). The interaction of the $O_2(^1\Delta_g)$ and KI due to light activation of PSs produces biocidal I_2 or I_3^-, which allow to increase cell damage. Consequently, this alternative pathway of cytotoxicity potentiated by KI allows to enhance the PDI of bacteria sensitized by **MePyridyl-DPP**.

In several cases, *S. aureus* bacterial infections are associated with the formation of biofilms (55). Therefore, the most effective DPP to eliminate planktonic cells was evaluated as photosensitizing agent on biofilms. For this purpose, *S. aureus* cells were incubated overnight with shaking at 37°C and the biofilm was formed on an acrylic disc. In general, the initial phase of biofilm formation reveals a degree of adhesion with fewer cells evenly distributed (56,57). After overnight incubation, the *S. aureus* biofilm structure exhibits a higher number of intimately packed bacterial cells, although the acrylic disc was not completely covered with cells and with low amount of extracellular matrix (33). In these experiments, the concentration of **MePyridyl-DPP** was increased to 5 μM and the irradiation conditions were kept as in the cell suspensions. The results are shown in Fig. 9. No toxicity was observed in biofilm cells treated with PS and kept in the dark. The inactivation of *S. aureus* was dependent on the irradiation time. A low inactivation was found with only 5 min of

irradiation. When the exposure period was extended to 15 min, the photodynamic effect produced a 2 $\log_{10}$ decrease in cell viability. Moreover, a reduction in cell survival of 4.5 $\log_{10}$ was reached upon 30 min of irradiation. Under the last conditions, 99.99% of the *S. aureus* cells were inactivated on the biofilm. Therefore, **MePyridyl-DPP** was also an active PS to inactivate *S. aureus*, even when the cells are integrated into a community of bacteria that grow embedded in a matrix to form biofilms.

<Figure 8>

<Figure 9>

CONCLUSIONS

DPP derivatives substituted by sulfonamide, pyridyl and *N*-methylpyridyl groups were evaluated as PSs to inactivate *S. aureus*. Spectroscopic characterizations showed that **Sulfonamide-DPP** and **Dipyridyl-DPP** have an intense absorption band centered at about 480 nm, while in **MePyridyl-DPP** this band was bathochromically shifted at 506 nm. Non-charged compounds showed green light emission with high Φ_F values in ACN. However, dicationic DPP produced red light emission with a decreased in Φ_F of 3.5 times. Moreover, large Stokes shifts were found for **Sulfonamide-DPP** and **Dipyridyl-DPP** and it increased in **MePyridyl-DPP**. This behavior can be caused by the different geometry of the DPPs in the S_0 and in S_1 states, which was also accompanied by the change in electron density distribution in S_1 compared to S_0. Photodynamic activity sensitized by DPPs exhibited the generation of $O_2(^1\Delta_g)$ in the organic solvent. In addition, the formation of $O_2^{\cdot-}$ induced by these compounds was similar to that of the control in the presence of NADH. However, the production of ROS can be modified in a microheterogenic environment, such as that found in the walls of microbial cells. Furthermore, the capacity of the DPPs to photoinactivate *S. aureus in vitro* was compared. A high photodamage induced by **MePyridyl-DPP** was observed at single-bacterium level of *S. aureus* cells attached to a surface. Furthermore, this dicationic PS was able to produce a complete elimination of cell suspensions after 30 min irradiation. Also, the same effect in planktonic

S. aureus cells was possible by potentiation of **MePyridyl-DPP** with KI and irradiation for 15 min. This result shows that KI can increase strongly the photoinactivation of bacteria even using PSs with low $O_2(^1\Delta_g)$ production. Possibly, the potentiation induced by this inorganic salt involves a combination of external heavy atom effect and the production of reactive iodine species. Also, dicationic DPP was able to photoinactivate bacterial cells on biofilms. In particular, the two positive charges at the periphery of **MePyridyl-DPP** can facilitate its interaction with the bacteria cell envelope. Therefore, this dicationic amphiphilic structure combined with iodide anions make this DPP an effective PS to eliminate *S. aureus*.

Acknowledgements. This work was supported by ANPCYT (PICT 02391/19), CONICET (PIP 2021-23 PIP 11220200101208CO) and UNRC-SECYT (PPI-2020). Thanks are due to Fundação para a Ciência e a Tecnologia (FCT) for the financial support to LAQV-REQUIMTE (UIDB/50006/2020) through national funds and, where applicable, co-financed by FEDER, within the PT2020 Partnership Agreement, and to the Portuguese NMR Network. J.E.D., N.S.G., A.M.D. and E.N.D. are Scientific Members of CONICET. M.E.P. thanks CONICET for the research fellowship. V.A.S.A. thanks FCT for his doctoral grant (SFRH/BD/135598/2018).

SUPPORTING INFORMATION

Additional supporting information may be found online in the Supporting Information section at the end of the article:

Section S1. Materials

Section S2. Instrumentation

Section S3. Computational details

Section S4. Growth conditions of microbial strains

Section S5. Statistical analysis

Section S6. Schemes and Figures

Section S7. NMR and MS spectra

Scheme S1. Synthesis of **Dipyridyl-DPP** and **MePyridyl-DPP** (5).

Scheme S2. Reaction of $O_2(^1\Delta_g)$ with iodide anions in aqueous media (6).

Figure S1. Absorption spectral changes during the photooxidation of DMA sensitized by (A) **Sulfonamide-DPP**, (B) **Dipyridyl-DPP** and (C) **MePyridyl-DPP** in ACN at different irradiation times (Δt = 60 s), λ_{irr} = 523 nm.

Figure S2. Absorption spectra changes of NBT photoreduction mediated by (A) **Sulfonamide-DPP**, (B) **Dipyridyl-DPP** and (C) **MePyridyl-DPP** in DMF after different irradiation times (Δt = 60 s). Control of (D) NBT and NADH without DPP, [NBT] = 0.2 mM and [NADH] = 0.5 mM, λ_{irr} = 523 nm.

Figure S3. Optimized structures of DPPs obtained by DFT at the CAM-B3LYP/6–31G(d) level using Gaussian 09. Blue arrow indicates the calculated relative magnitude and orientation of permanent dipole moment (μ).

Figure S4. (A) Absorption and (B) fluorescence emission (λ_{exc} = 523 nm) spectra of **Sulfonamide- DPP** (green), **Dipyridyl-DPP** (red) and **MePyridyl-DPP** (blue) in DMF.

Figure S5. Overlap of optimized geometries of S_0 (balls and sticks) and relaxed S_1 (sticks) at the CAM-B3LYP/6–31G(d) level using Gaussian 09.

Figure S6. First-order plots for the photooxidation of DMA sensitized by **MePyridyl-DPP** (▲) and Rose bengal (●) in methanol, λ_{irr} = 523 nm.

Figure S7. Survival curves of *S. aureus* (~10^8 CFU/mL) treated with 2 μM DPP for 30 min in the dark at 37 °C and kept in the dark for different times. **Sulfonamide-DPP** (▼), Dipyridyl-DPP (■) and **MePyridyl-DPP** (▲).

Figure S8. Survival curves of *S. aureus* (~10^8 CFU/mL) treated with 50 mM KI for 10 min and 2 μM DPP for 30 min in the dark at 37 °C and kept in the dark for different times. **Sulfonamide-DPP** (▼), Dipyridyl-DPP (■) and MePyridyl-DPP (▲).

REFERENCES

1. Pham, T. C., Nguyen, V.-N., Choi, Y., Lee, S. and J. Yoon (2021) Recent strategies to develop innovative photosensitizers for enhanced photodynamic therapy. *Chem. Rev.* **121**, 13454-13619.
2. Youf, R., Müller, M., Balasini, A., Thétiot, F., Müller, M., Hascoët, A., Jonas, U., Schönherr, H., Lemercier, G., Montier, T. and T. Le Gall (2021) Antimicrobial photodynamic therapy: latest developments with a focus on combinatory strategies. *Pharmaceutics* **13**, 1995.
3. Hamblin, M. R. and H. Abrahamse (2020) Oxygen-independent antimicrobial photoinactivation: type III photochemical mechanism? *Antibiotics* **9**, 53.
4. Marasini, S., Leanse, L. G. and T. Dai (2021) Can microorganisms develop resistance against light based anti-infective agents? *Adv. Drug Deliv. Rev.* **175**, 113822.
5. Alves, E., Faustino, M. A. F., Neves, M. G. P. M. S., Cunha, Â., Nadais, H. and A. Almeida (2015) Potential applications of porphyrins in photodynamic inactivation beyond the medical scope. *J. Photochem. Photobiol. C: Photochem. Rev.* **22**, 34-57.
6. Ribeiro, C. P. S. and L. M. O. Lourenço (2021) Overview of cationic phthalocyanines for effective photoinactivation of pathogenic microorganisms. *J. Photochem. Photobiol. C: Photochem. Rev.* **48**, 100422.
7. Lo, P.-C., Rodríguez-Morgade, M. S., Pandey, R. K., Ng, D. K. P., Torres T. and F. Dumoulin (2020) The unique features and promises of phthalocyanines as advanced photosensitisers for photodynamic therapy of cancer. *Chem. Soc. Rev.* **49**, 1041-1056.
8. Spesia, M. B. and E. N. Durantini (2022) Evolution of phthalocyanine structures as photodynamic agents for bacteria inactivation. *Chem. Rec.* **22**, e202100292.
9. Heredia, D. A., Durantini, A. M., Durantini, J. E. and E. N. Durantini (2022) Fullerene C_{60} derivatives as antimicrobial photodynamic agents. *J. Photochem. Photobiol. C: Photochem. Rev.* **51**, 100471.
10. Durantini, A. M., Heredia, D. A., Durantini, J. E. and E. N. Durantini (2018) BODIPYs to the rescue: potential applications in photodynamic inactivation. *Eur. J. Med. Chem.* **144**, 651-661.
11. Agazzi, M. L., Ballatore, M. B., Durantini, A. M., Durantini, E. N. and A. C. Tomé (2019)

BODIPYs in antitumoral and antimicrobial photodynamic therapy: an integrating review. *J. Photochem. Photobiol. C: Photochem. Rev.* **40**, 21-48.

12. Grzybowski, M. and D. T. Gryko (2015) Diketopyrrolopyrroles: synthesis, reactivity, and optical properties. *Adv. Optical Mater.* **3**, 280-320.
13. Kaur, M. and D. H. Choi (2015) Diketopyrrolopyrrole: brilliant red pigment dye-based fluorescent probes and their applications. *Chem. Soc. Rev.* **44**, 58-77.
14. Li, W., Wang, L., Tang, H. and D. Cao (2019) Diketopyrrolopyrrole-based fluorescent probes for detection and bioimaging: current progresses and perspectives. *Dyes Pigm.* **162**, 934-950.
15. Zheng, L., Li, J., Yu, M., Jia, W., Duan, S., Cao, D., Ding, X., Yu, B., Zhang, X. and F.-J. Xu (2020) Molecular sizes and antibacterial performance relationships of flexible ionic liquid derivatives. *J. Am. Chem. Soc.* **142**, 20257-20269.
16. Jiang, X., Wang, L., Tang, H., Cao, D. and W. Chen (2020) Diketopyrrolopyrrole: an emerging phototherapy agent in fighting cancer. *Dyes Pigm.* **181**, 108599.
17. Zhang, Q., Wang, Q., Xu, X., Liu, J., Lu, X., Huang, W. and Q. Fan (2021) Diketopyrrolopyrrole derivatives-based NIR-II fluorophores for theranostics. *Dyes Pigm.* **193**, 109480.
18. Zhang, H., Liang, Y., Zhao, H., Qi, R., Chen, Z., Yuan, H., Liang, H. and L. Wang (2020) Dual-mode antibacterial conjugated polymer nanoparticles for photothermal and photodynamic therapy. *Macromol. Biosci.* **20**, 1900301.
19. Du, Y., Liu, X., Wang, Q., Yu, L., Chu, L. and M. Sun (2022) Metal free benzothiadiazole-diketopyrrolopyrrole-based conjugated polymer/g-C_3N_4 photocatalyst for enhanced sterilization and degradation in visible to near-infrared region. *J. Colloid Interface Sci.* **608**, 103-113.
20. Agazzi, M. L., Almodovar, V. A. S., Gsponer, N. S., Bertolotti, S., Tomé, A. C. and E. N. Durantini (2020) Diketopyrrolopyrrole-fullerene C_{60} architectures as highly efficient heavy atom-free photosensitizers: synthesis, photophysical properties and photodynamic activity. *Org. Biomol. Chem.* **18**, 1449-1461.
21. Baigorria, E., Durantini, J. E., Di Palma, M. A., Gsponer, N. S., Milanesio, M. E. and E. N.

Durantini (2021) Amphiphilic tricationic Zn(II)phthalocyanine provides effective photodynamic action to eradicate broad-spectrum microorganisms. *Photochem. Photobiol. Sci.* **20**, 939-953.

22. Agazzi, M. L., Durantini, J. E., Quiroga, E. D., Alvarez, M. G. and E. N. Durantini (2021) A novel tricationic fullerene C_{60} as broad-spectrum antimicrobial photosensitizer: mechanisms of action and potentiation with potassium iodide. *Photochem. Photobiol. Sci.* **20**, 327-341.
23. Ramos, C. I. V., Almodôvar, V. A. S., Candeias, N. R., Santos, T., Cruz, C., Neves, M. G. P. M. S. and A. C. Tomé (2022) Diketopyrrolo[3,4-c]pyrrole derivative as a promising ligand for the stabilization of G-quadruplex DNA structures. *Bioorg. Chem.* **122**, 105703.
24. Shankar, N., Soe, P.-m. and C. C. Tam (2020) Prevalence and risk of acquisition of methicillin-resistant *Staphylococcus aureus* among households: a systematic review. *Int. J. Infect. Dis.* **92**, 105-113.
25. Zhou, S.,Rao, Y., Li, J., Huang, Q. and X. Rao (2022) *Staphylococcus aureus* small-colony variants: formation, infection, and treatment. *Microbiol. Res.* 260, 127040.
26. Pop, F., Humphreys, J., Schwarz, J., Brown, L., Berg, A. van den and D. B. Amabilino (2019) Towards more sustainable synthesis of diketopyrrolopyrroles. *New J. Chem.* 43, 5783-5790.
27. Durantini, A. M., Greene, L. E., Lincoln, R., Martínez, S. R. and G. Cosa (2016) Reactive oxygen species mediated activation of a dormant singlet oxygen photosensitizer: from autocatalytic singlet oxygen amplification to chemicontrolled photodynamic therapy. *J. Am. Chem. Soc.* **138**, 1215-1225.
28. Gollnick, K. and G. O. Shenck (1964) Mechanism and stereoselectivity of photosensitized oxygen transfer reactions. *Pure Appl. Chem.* **9**, 507-525.
29. Martínez, S. R., Palacios, Y. B., Heredia, D. A., Agazzi, M. L. and A. M. Durantini (2019) Phenotypic resistance in photodynamic inactivation unravelled at the single bacterium level. *ACS Infect. Dis.* **5**, 1624-1633.
30. Scanone, A. C., Gsponer, N. S., Alvarez, M. G., Heredia, D. A., Durantini, A. M. and E. N. Durantini (2020) Magnetic nanoplatforms for *in situ* modification of macromolecules: synthesis,

characterization, and photoinactivating power of cationic nanoiman-porphyrin conjugates. *ACS Appl. Bio Mater.* **3**, 5930-5940.

31. Pérez, M. E., Durantini, J. E., Reynoso, E., Alvarez, M. G., Milanesio, M. E. and E. N. Durantini (2021) Porphyrin-Schiff base conjugates bearing basic amino groups as antimicrobial phototherapeutic agents *Molecules* **26**, 5877.
32. Santamarina, S. C., Heredia, D. A., Durantini, A. M. and E. N. Durantini (2022) Antimicrobial photosensitizing material based on conjugated Zn(II) porphyrins. *Antibiotics* **11**, 91.
33. Mamone, L., Ferreyra, D. D., Gándara, L., Di Venosa, G., Vallecorsa, P., Sáenz, D., Calvo, G., Batlle, A., Buzzola, F., Durantini, E. N. and A. Casas (2016) Photodynamic inactivation of planktonic and biofilm growing bacteria mediated by a meso-substituted porphyrin bearing four basic amino groups. *J. Photochem. Photobiol. B: Biol.* **161**, 222-229.
34. Colonna, G., Pilati, T., Rusconi, F. and G. Zecchi (2007) Synthesis and properties of some new *N*,*N*'-disubstituted 2,5-dihydro-1,4-dioxo-3,6-diphenylpyrrolo[3,4-c]pyrroles. *Dyes Pigm.* **75**, 125-129.
35. Aigner, D., Ungerbock, B., Mayr, T., Saf, R., Klimant, I. and S. M. Borisov (2013) Fluorescent materials for pH sensing and imaging based on novel 1,4-diketopyrrolo[3,4-c]pyrrole dyes. *J. Mater. Chem. C* **1**, 5685-5693.
36. Almodovar, V. A. S. and A. C. Tomé (2021) A convenient synthesis of diketopyrrolopyrrole dyes. *Molecules* 26, 4758-12766.
37. Cai, Y., Liang, P., Si, W., Zhao, B., Shao, J., Huang, W., Zhang, Y., Zhang, Q. and X. Dong (2018) A selenophene substituted diketopyrrolopyrrole nanotheranostic agent for highly efficient photoacoustic/infrared-thermal imaging-guided phototherapy. *Org. Chem. Front.* **5**, 98-105.
38. Gsponer, N. S., Agazzi, M. L., Spesia, M. B. and E. N. Durantini (2016) Approaches to unravel pathways of reactive oxygen species in the photoinactivation of bacteria induced by a dicationic fulleropyrrolidinium derivative. *Methods* **109**, 167-174.
39. Reynoso, E., Quiroga, E. D., Agazzi, M. L., Ballatore, M. B., Bertolotti, S. G. and E. N. Durantini

(2017) Photodynamic inactivation of microorganisms sensitized by cationic BODIPY derivatives potentiated by potassium iodide. *Photochem. Photobiol. Sci.* **16**, 1524-1536.

40. Shi, H., Sun, W., Wang, Q., Gu, G., Si, W., Huang, W., Zhang Q. and X. Dong (2016) A thienyl-substituted diketopyrrolopyrrole derivative with efficient reactive oxygen species generation for photodynamic therapy. *ChemPlusChem* **81**, 515-520.
41. Danne, C. and S. Dramsi (2012) Pili of Gram-positive bacteria: roles in host colonization. *Res. Microbiol.* **163**, 645-658.
42. Samanta, A., Paul, B. K. and N. Guchhait (2012) Photophysics of DNA staining dye propidium iodide encapsulated in bio-mimetic micelle and genomic fish sperm DNA. *J. Photochem. Photobiol. B: Biol.* **109**, 58-67.
43. Duedu, K. O. and C. E. French (2017) Two-colour fluorescence fluorimetric analysis for direct quantification of bacteria and its application in monitoring bacterial growth in cellulose degradation systems. *J. Microbiol. Methods* **135**, 85-92.
44. Scanone, A. C., Santamarina, S. C., Heredia, D. A., Durantini, E. N. and A. M. Durantini (2020) Functionalized magnetic nanoparticles with BODIPYs for bioimaging and antimicrobial therapy applications. *ACS Appl. Bio Mater.* **3**, 1061-1070.
45. Guzmán-Soto, I., McTiernan, C., Gonzalez-Gomez, M., Ross, A., Gupta, K., Suuronen, E. J., Mah, T.-F., Griffith, M. and E. I. Alarcon (2021) Mimicking biofilm formation and development: recent progress in in vitro and in vivo biofilm models. *iScience* **24**, 102443.
46. Agazzi, M. L., Ballatore, M. B., Reynoso, E., Quiroga, E. D. and E. N. Durantini (2017) Synthesis, spectroscopic properties and photodynamic activity of two cationic BODIPY derivatives with application in the photoinactivation of microorganisms. *Eur. J. Med. Chem.* **126**, 110-121.
47. Hamblin M. R. (2017) Potentiation of antimicrobial photodynamic inactivation by inorganic salts *Expert. Rev. Anti Infect. Ther.* **15**, 1059-1069.
48. Vecchio, D., Gupta, A., Huang, L., Landi, G., Avci, P., Rodas, A. and M. R. Hamblin (2015) Bacterial photodynamic inactivation mediated by methylene blue and red light is enhanced by

synergistic effect of potassium iodide. *Antimicrob. Agents Chemother.* 59, 5203-5212.

49. Zhang, Y., Dai, T., Wang, M., Vecchio, D., Chiang, L.Y. and M. R. Hamblin (2015) Potentiation of antimicrobial photodynamic inactivation mediated by a cationic fullerene by added iodide: *in vitro* and *in vivo* studies. *Nanomedicine* **10**, 603-614.
50. Huang, L., Szewczyk, G., Sarna, T. and M. R. Hamblin (2017) Potassium iodide potentiates broad-spectrum antimicrobial photodynamic inactivation using Photofrin. *ACS Infect. Dis.* **3**, 320-328.
51. Huang, L., El-Hussein, A., Xuan, W. and M. R. Hamblin (2018) Potentiation by potassium iodide reveals that the anionic porphyrin $TPPS_4$ is a surprisingly effective photosensitizer for antimicrobial photodynamic inactivation. *J. Photochem. Photobiol. B: Biol.* **178**, 277-286.
52. Ladeira, B. M. F., Dias, C. J., Gomes, A. T. P. C., Tomé, A. C., Neves, M. G. P. M. S., Moura, N. M. M., Almeida, A. and M. A. F. Faustino (2021) Cationic pyrrolidine/pyrroline-substituted porphyrins as efficient photosensitizers against *E. coli*. *Molecules* **26**, 464.
53. Chmyrov, A., Sanden T. and J. Widengren (2010) Iodide as a fluorescence quencher and promoters-mechanisms and possible implications. *J. Phys. Chem. B* **114**, 11282-11291.
54. Vieira, C., Gomes, A. T. P. C., Mesquita, M. Q., Moura, N. M. M., Neves, M. G. P. M. S., Faustino, M. A. F. and A. Almeida (2018) An insight into the potentiation effect of potassium iodide on aPDT efficacy. *Frontiers Microbiol.* **9**, 2665.
55. Silva, R. A. G., Afonina, I. and K. A. Kline (2021) Eradicating biofilm infections: an update on current and prospective approaches. *Curr. Opin. Microbiol.* **63**, 117-125.
56. Zago, C. E., Silva, S., Sanitá, P. V., Barbugli, P. A., Dias, C. M. I., Lordello, V. B. and C. E. Vergani (2015) Dynamics of biofilm formation and the interaction between *Candida albicans* and Methicillin-Susceptible (MSSA) and -Resistant *Staphylococcus aureus* (MRSA). *PLoS One* **10**, e0123206.
57. Trotonda, M. P., Tamber, S., Memmi, G. and A. L. Cheung (2008) MgrA represses biofilm formation in *Staphylococcus aureus*. *Infect. Immun.* **76**, 5645-5654.

FIGURE CAPTIONS

Scheme 1. Structures of DPP derivatives.

Scheme 2. Synthesis of **Sulfonamide-DPP**.

Figure 1. Optimized structure and the ESP surfaces of DPPs calculated for ground state by using DFT at the CAM-B3LYP/6-31G(d) level. Created with GaussView Software founded on Gaussian 09 calculations. The positive ESP regions are colored blue and the negative ones red.

Figure 2. (A) Absorption and (B) fluorescence emission (λ_{exc} = 483 nm) spectra of **Sulfonamide-DPP** (green), **Dipyridyl-DPP** (red) and **MePyridyl-DPP** (blue) in ACN.

Figure 3. Highest occupied molecular orbital (HOMO) and lowest unoccupied molecular orbital (LUMO) of DPPs. All calculations were performed by DFT at the CAM-B3LYP/6–31G(d) level using Gaussian 09.

Figure 4. First-order plots for the photooxidation of DMA sensitized by **Sulfonamide-DPP** (▾), **Dipyridyl-DPP** (■), **MePyridyl-DPP** (▲) and **Br_2B-OAc** (●) in ACN, λ_{irr} = 523 nm.

Figure 5. Time course of $O_2^{\bullet-}$ formation detected by the NBT reduction in the presence of NADH sensitized by **Sulfonamide-DPP** (▾), **Dipyridyl-DPP** (■) and **MePyridyl-DPP** (▲) as an increase in the absorption at 560 nm in DMF. Control: NBT + NADH (●), [NBT] = 0.2 mM and [NADH] = 0.5 mM, λ_{irr} = 523 nm.

Figure 6. Microscopy images of *S. aureus* incubated with 2 μM DPP for 20 min in the dark and then irradiated with green light for different times; column A: cells under bright field; columns B: fluorescence emission of PI (scale bar 5 μm).

Figure 7. Survival curves of *S. aureus* (~10^8 CFU/mL) incubated with 2 μM DPP for 20 min in the dark at 37 °C and irradiated with green light for different periods. **Sulfonamide-DPP** (▾), **Dipyridyl-DPP** (■), **MePyridyl-DPP** (▲) and irradiated control culture without DPP (●).

Figure 8. Survival curves of *S. aureus* (~10^8 CFU/mL) treated with 50 mM KI for 10 min and 2 μM DPP for 20 min in the dark at 37 °C and irradiated with green light for different times. **Sulfonamide-DPP** (▾), **Dipyridyl-DPP** (■), **MePyridyl-DPP** (▲) and irradiated control culture without DPP (●).

Figure 9. Survival of *S. aureus* biofilms incubated with 5 μM **MePyridyl-DPP** for 20 min in the dark at 37 °C and irradiated with green light for different times; (1) control in the dark, (2) 5 μM PS in the dark, (3) 5 μM PS and 5 min irradiation, (4) 5 μM PS and 15 min irradiation, (5) 5 μM PS and 30 min irradiation.

Table 1. Spectroscopic properties of DPPs in ACN.

DPP	λ_{max}^{abs} (nm)		λ_{max}^{em} (nm)	Φ_F[a]
Sulfonamide-DPP	282	478	554	0.79 ± 0.02
Dipyridyl-DPP	292	482	562	0.77 ± 0.02
MePyridyl-DPP	320	506	645	0.18 ± 0.01

[a] Fluorescence quantum yield, reference **H_2B-OAc** Φ_F = 0.87 (27).

Table 2. Kinetic parameters for the photooxidation reaction of DMA (k_{obs}^{DMA}) sensitized by DPPs and quantum yields of $O_2(^1\Delta_g)$ production (Φ_Δ) in ACN.

DPP	Solvent	k_{obs}^{DMA} (s^{-1})	Φ_Δ
Sulfonamide-DPP	ACN	(3.98 ± 0.06) x 10^{-4}	0.17±0.02 [a]
Dipyridyl-DPP	ACN	(3.42 ± 0.05) x 10^{-4}	0.15±0.02 [a]
MePyridyl-DPP	ACN	(2.28 ± 0.06) x 10^{-5}	0.010±0.004 [a]
MePyridyl-DPP	methanol	(1.12 ± 0.03) x 10^{-5}	0.16±0.02 [b]

[a] reference **Br_2B-OAc**, k_{obs}^{DMA} = (1.85 ± 0.02) x 10^{-3} s^{-1}, Φ_Δ = 0.79 (27); reference Rose bengal, k_{obs}^{DMA} = (5.46 ± 0.04) x 10^{-5} s^{-1}, Φ_Δ = 0.76 (28).

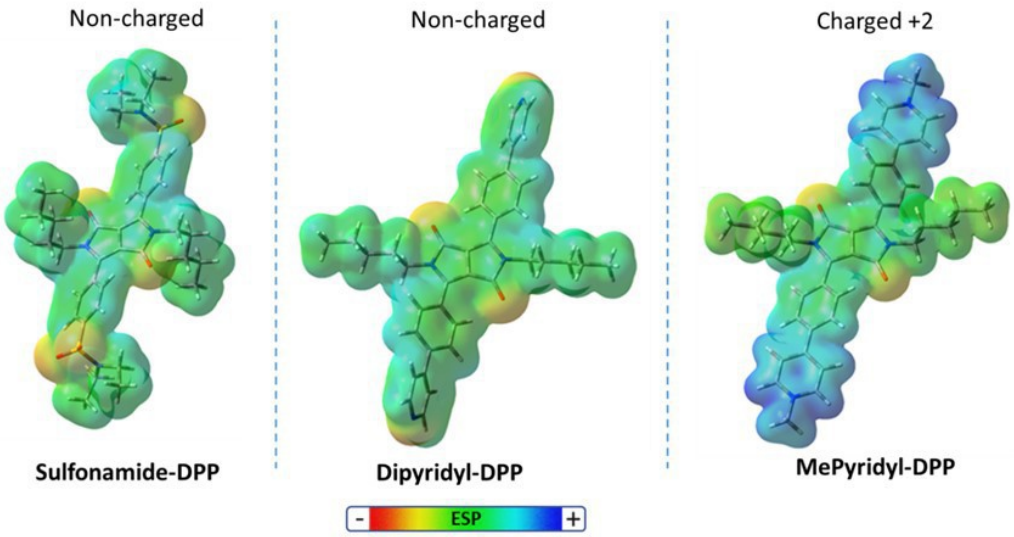

Figure 1

PHP_13741_Figure 1.JPG

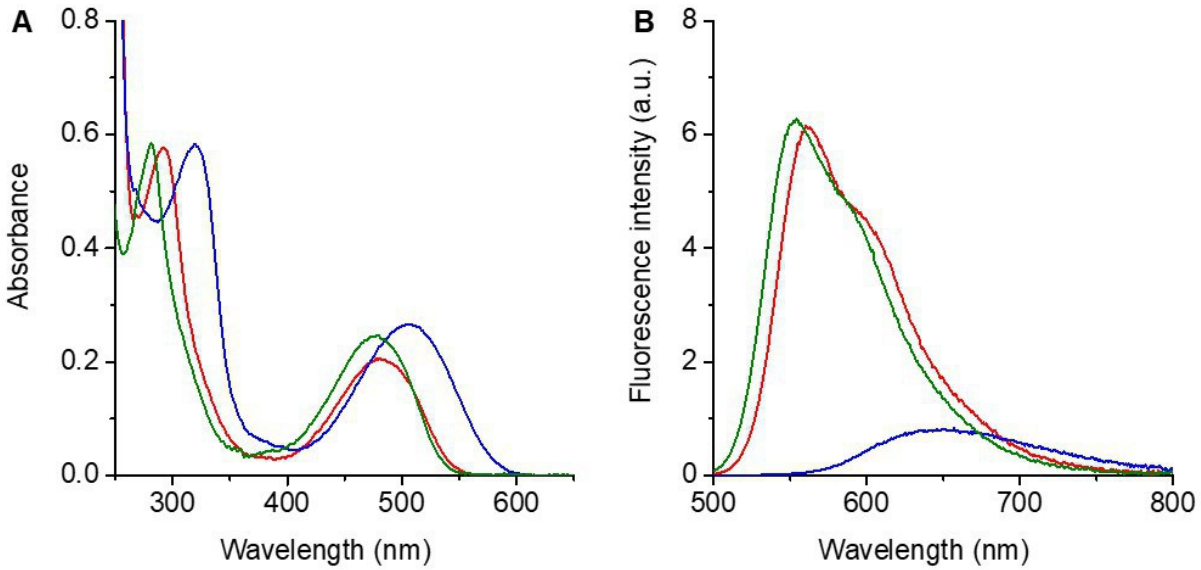

Figure 2

PHP_13741_Figure 2.JPG

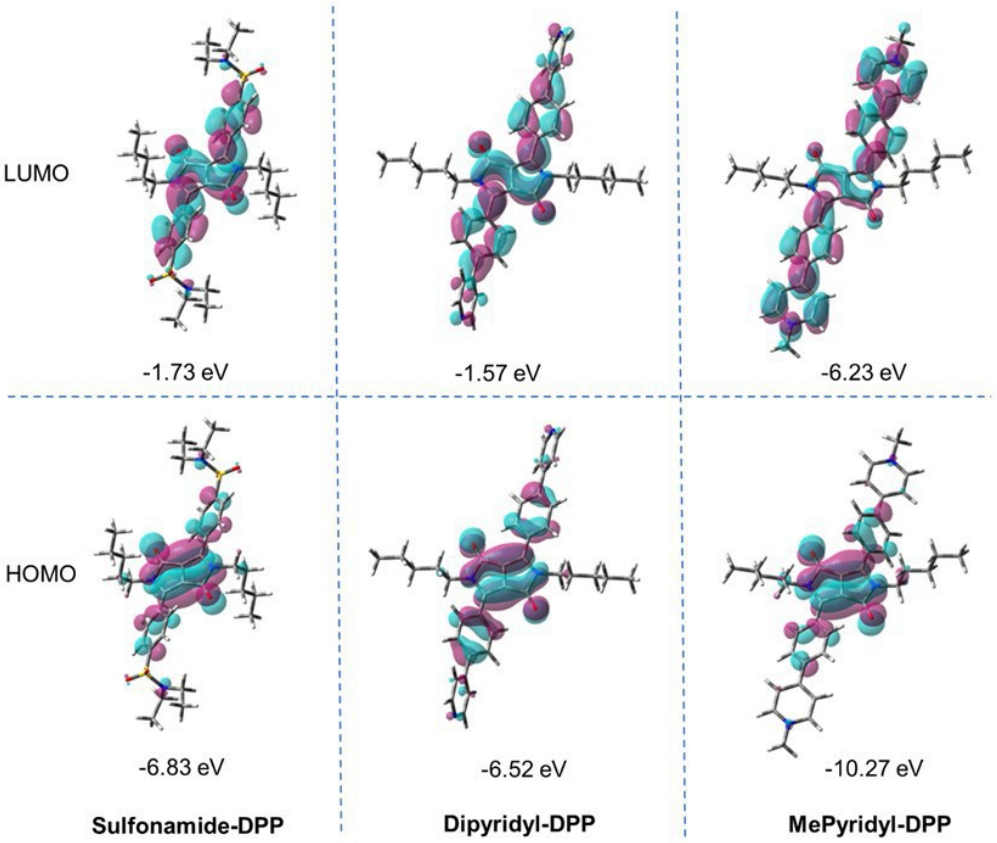

Figure 3

PHP_13741_Figure 3.JPG

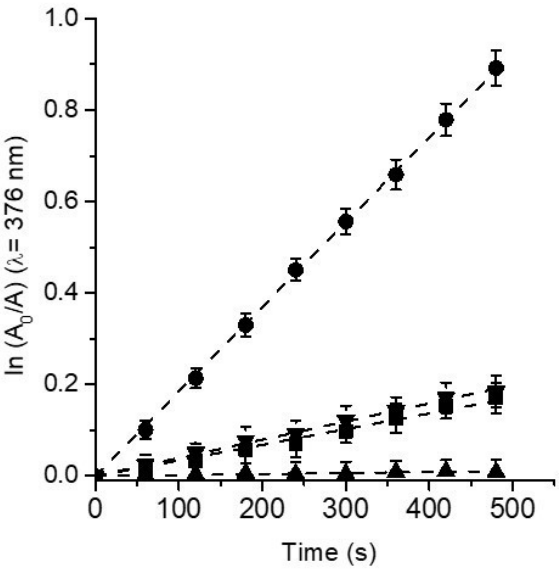

Figure 4

PHP_13741_Figure 4.JPG

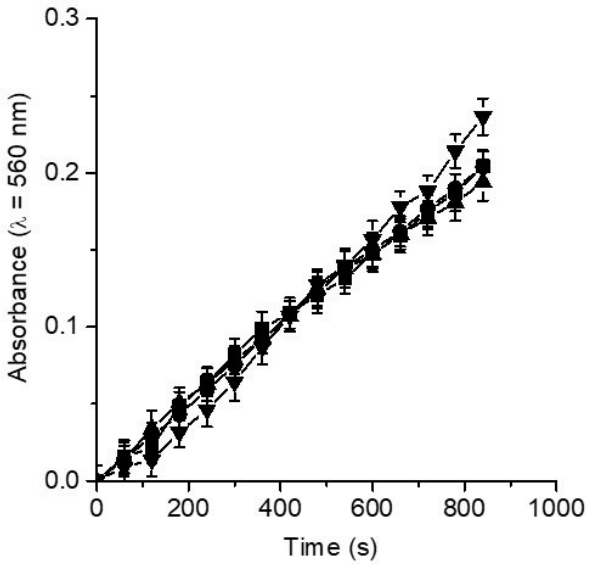

Figure 5

PHP_13741_Figure 5.JPG

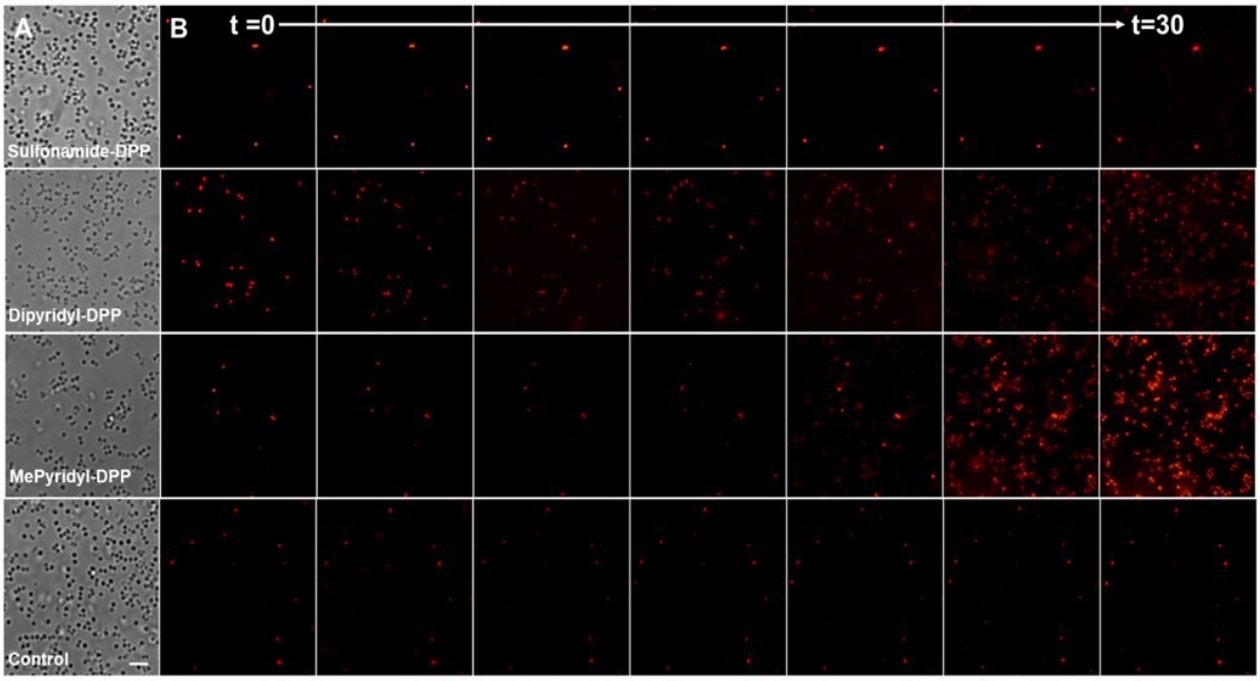

Figure 6

PHP_13741_Figure 6.JPG

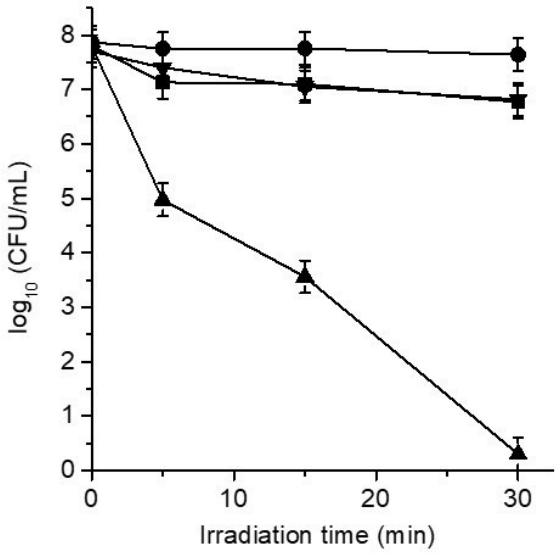

Figure 7

PHP_13741_Figure 7.JPG

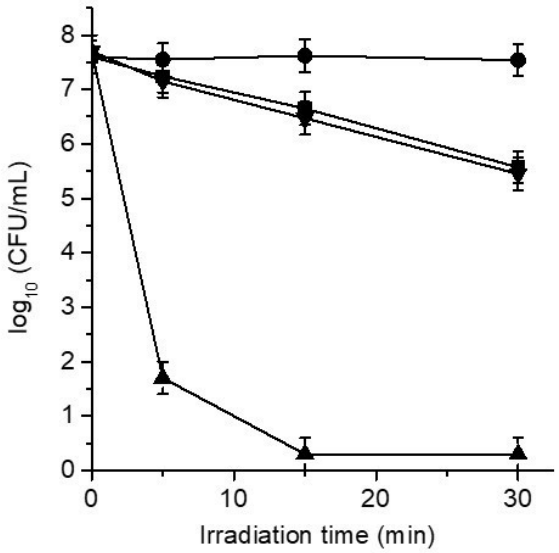

Figure 8

PHP_13741_Figure 8.JPG

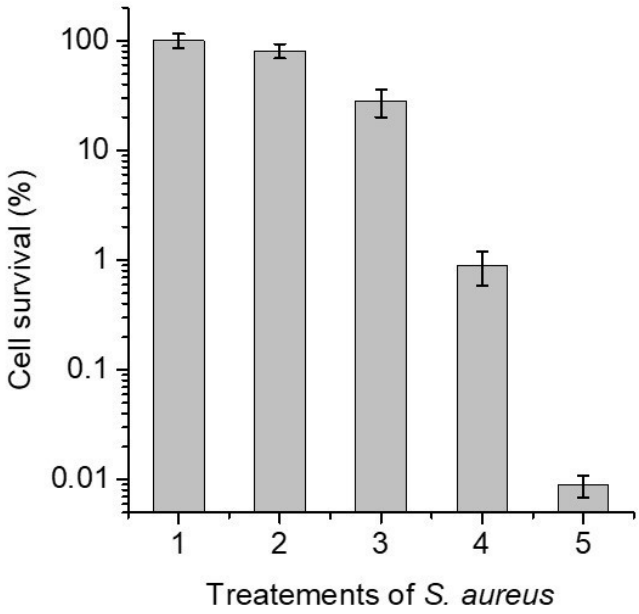

Figure 9

PHP_13741_Figure 9.JPG

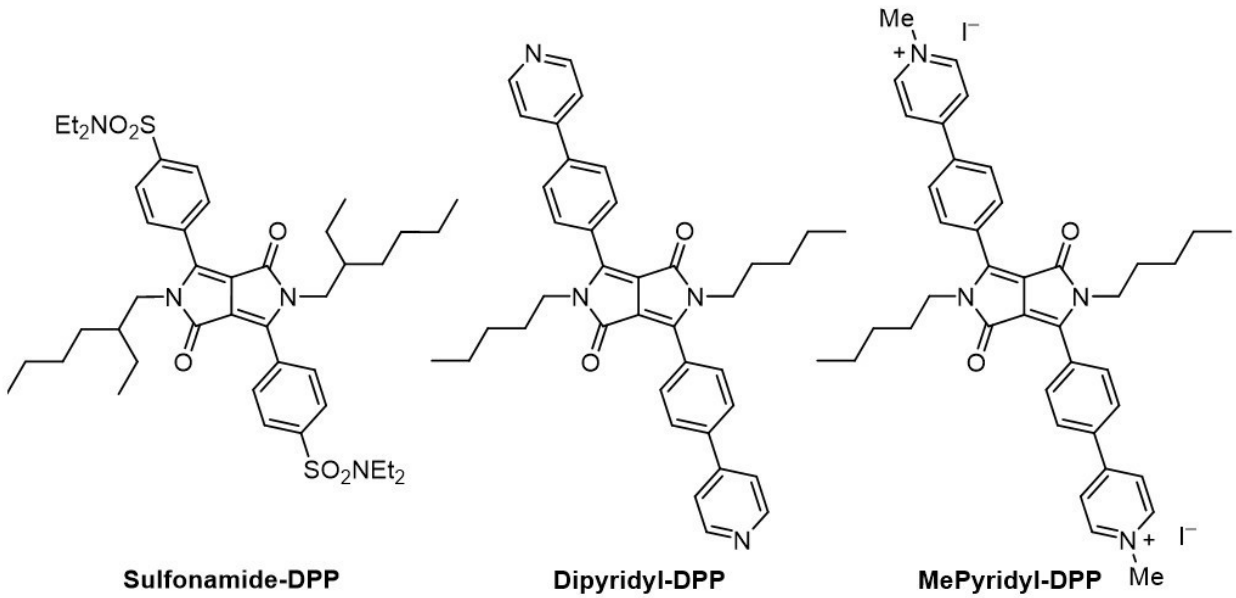

Scheme 1

PHP_13741_Scheme 1.JPG

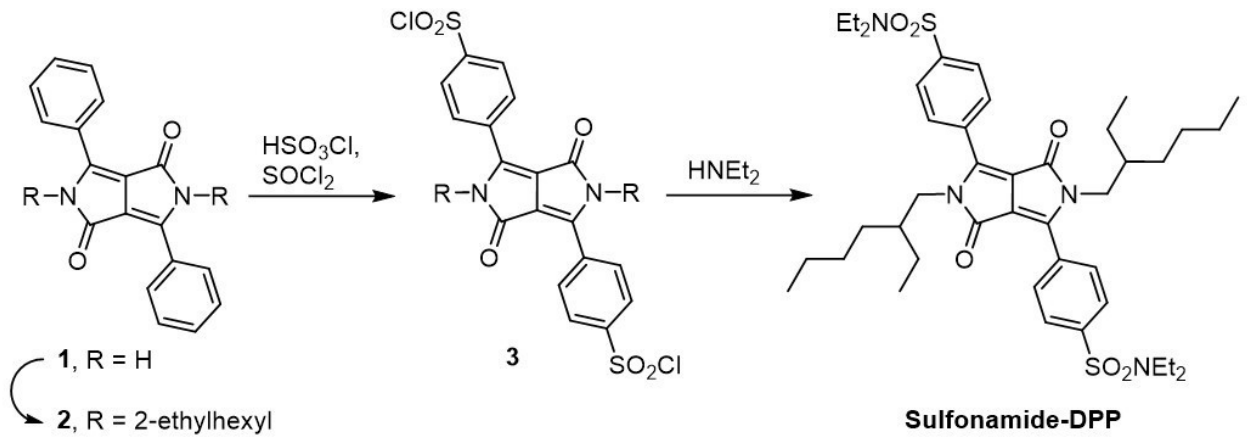

Scheme 2

PHP_13741_Scheme 2.JPG